Contents lists available at ScienceDirect

Transactions of Nonferrous Metals Society of China

36(2026) 586−599

www.tnmsc.cn

Effects of modulation layer thickness on microstructures and mechanical behavior of VN/TiN−Ni nano-multilayered films

Wen-jie CHENG [a,b], Ping LIU [b], Xin-fa ZHU [c], Yi MENG [c], Hong-mei LU [c], Peter K. LIAW [d], Wei LI [b,*]

[a] Center for Research on the Preparation and Properties of New Functional Materials, School of Physics and Electronic Engineering, Hanjiang Normal University, Shiyan 442000, China;

[b] School of Materials and Chemistry, University of Shanghai for Science and Technology, Shanghai 200093, China;

[c] Shanghai Tool Factory Company Limited, Shanghai 200093, China;

[d] Department of Materials Science and Engineering, The University of Tennessee, Knoxville TN 37996, USA

Abstract: The dependence of interface structure and mechanical properties on the modulation layer thickness of VN/TiN−Ni nano-multilayered films deposited on Si substrates using a reactive magnetron sputtering technique was systematically investigated. The films were characterized using X-ray diffraction, scanning electron microscopy, X-ray photoelectron spectroscopy, transmission electron microscopy, and nanoindentation. The results show that the TiN−Ni layer grows epitaxially on the VN layer, forming a coherent interface between the two sublayers. When the deposition time ratio of the two sublayers (T_{TiN-Ni}:T_{VN}) is 10:12, the films exhibit remarkable mechanical properties, with hardness, elastic modulus, and fracture toughness values of 25.9 GPa, 317 GPa, and 1.88 MPa·m$^{1/2}$, respectively. Meanwhile, fracture toughness is improved by approximately 50% compared to the VN monolithic film. This enhancement is attributed to the coherent interface between the sublayers and the phase separation in the TiN−Ni layer.

Keywords: nano-multilayered film; modulation-layer thickness; phase separation; strengthening; fracture toughness

1 Introduction

Nanostructured nitride films, such as vanadium nitride (VN) and titanium nitride (TiN), are increasingly employed in the machining and forming tool industries because of their excellent hardness, thermal stability, and wear resistance [1−3]. However, since hardness and fracture toughness are typically inversely related, the low intrinsic fracture toughness of these films limits their practical applications [4,5]. As a result, considerable research has focused on overcoming this trade-off [6,7].

In nano-multilayered films, the thickness of individual layers plays a crucial role in determining the properties of each constituent layer. Consequently, the characteristics of each layer and the thickness of the bilayer unit are key factors in determining the overall properties of the final films [8,9]. Furthermore, the nano-multilayered structure can hinder columnar grain growth and combine the advantages of each sublayer. These films often exhibit significant improvements in mechanical properties compared to monolithic films, owing to the interface structures and the complex interactions between the layers [10–12]. For example, PAN et al [13] fabricated VN/TiB_2 nano-multilayered films with different modulation ratios (t_{VN}:t_{TiB_2}) using magnetron sputtering. When the ratio was 1:7, the films displayed remarkable hardness and elastic modulus of 41.8 GPa and 492.4 GPa, respectively. The molecular dynamics simulations were also

Corresponding author: *Wei LI, Tel: +86-21-55271670, E-mail: liwei176@usst.edu.cn

https://doi.org/10.1016/S1003-6326(25)66983-4

Received 21 May 2024; accepted 8 January 2025

conducted to study V/VN nano-multilayered films with varying modulation periods [14]. The results showed that films with larger modulation period (Λ) values exhibited higher elastic modulus, greater elastic limits, and improved lattice integrity. Notably, strain hardening was observed when $\Lambda \geq 42.9$ Å. In another study, WANG et a [15] deposited monolithic AlCrSiN, VN, and AlCrSiN/VN nano-multilayered films using arc ion plating and magnetron sputtering. The nano-multilayered films demonstrated the highest hardness of 30.7 GPa, attributed to the interfacial enhancement mechanism and higher compressive stress. The interfacial structure of these multilayers was influenced by the modulation period and crystal structure, leading to significant improvements in mechanical properties compared to the monolithic films.

In addition to research focused on the hardness and strengthening mechanisms, the toughness and mechanisms of nano-multilayered films have also garnered increasing attention [16−18]. In these films, the interfacial structure between sublayers and the multicomponent phase transitions within the layers are considered key factor in enhancing toughness. DU et al [19] fabricated TiAlSiN/TiAlN multilayers with modulation ratios ranging from $t_{TiAlSiN}$:t_{TiAlN}=1:1 (ML) to $t_{TiAlSiN}$:t_{TiAlN}=1:2 (HML) using cathodic arc deposition. Their results showed that both ML and HML multilayers exhibited relatively weaker radial cracking and edge cracks in Vickers indentation tests compared to monolithic coatings. This was attributed to the bilayer interface acting as a barrier, preventing crack propagation and expansion under external stress. LORENTZON et al [20] produced TiN/$Zr_{0.37}Al_{0.63}N_{1.09}$ multilayer films with 10 nm in sublayer thickness by reactive DC magnetron sputtering at temperatures ranging from ambient to 900 °C. The films deposited at 200 and 900 °C exhibited the highest fracture toughness of (2.8±0.1) MPa·$m^{1/2}$. At lower temperatures, highly deformed w-$Zr_{0.37}Al_{0.63}N_{1.09}$ was formed, which improved fracture toughness by shielding crack tips due to differences in elastic modulus between the layers. ZHOU et al [21] prepared TiN/AlN−Ni multilayer films with varying modulated layer thicknesses using magnetron sputtering. The fracture toughness of these films reached a maximum value of 5.49 MPa·$m^{1/2}$. The enhanced toughness was attributed to an indentation-induced phase transition from c-AlN to w-AlN in AlN−Ni layer, leading to the formation of a finer, more coherent interface. These studies highlight how an appropriately designed interface structure can simultaneously enhance both the hardness and fracture toughness of nano-multilayered films. However, it is important to note that current research on the VN/TiN−Ni nano-multilayered system remains limited, and its potential for superior properties has less yet been fully explored.

In this study, VN with a face-centered cubic (FCC) structure was chosen as the template layer, while TiN and Ni metal were selected to form the composite modulation layer, with Ni acting as the separating phase. A series of VN/TiN−Ni nano-multilayered films with varying modulation layer thicknesses were prepared using reactive magnetron sputtering. The relationship among modulation layer thickness, interface structure, and mechanical properties of the VN/TiN−Ni nano-multilayered films was systematically investigated. Furthermore, the role of TiN−Ni phase separation in the toughening mechanism of the films was discussed.

2 Experimental

2.1 Film deposition

The VN/TiN−Ni nano-multilayered films were deposited on (100) silicon substrates (10 mm × 20 mm × 0.65 mm) using a reactive magnetron sputtering system (JGP−450), as illustrated in Fig. 1.

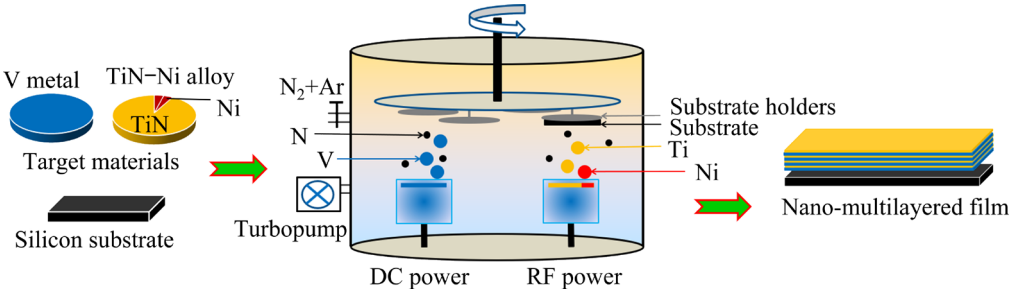

Fig. 1 Schematic diagram of high-vacuum dual-cathode magnetron sputtering system

The V metal target (99.99% in purity) was placed at the direct current (DC) cathode, while the TiN−Ni alloy target (99.99% in purity, with a TiN to Ni volume ratio of 23:2) was positioned at the radio frequency (RF) cathode. The deposition time ratio of TiN−Ni to VN (T_{TiN-Ni}:T_{VN}) was set to be 4:12, 6:12, 8:12, 10:12, and 12:12.

The silicon substrate was first cleaned with acetone and ethanol using ultrasonic waves for 20 min, then dried with high-purity N_2 gas (99.9999% in purity) and carefully placed on the substrate holder. The sputtering chamber was pumped down to 4×10^{-3} Pa, and argon gas (99.9999% in purity) was introduced for 15 min to clean the target surfaces. The substrate rotation speed was maintained at 3.8 r/min.

2.2 Characterization and test

The crystal structures of the VN/TiN−Ni nano-multilayered films were analyzed using X-ray diffraction technique (XRD, Bruker D8 Advance Diffractometer). The elemental composition was determined through electron probe microanalysis (EPMA, JXA−8530F PLUS). The bonding state and chemical composition were examined using X-ray photoelectron spectroscopy (XPS, Thermo Fisher Scientific K_α system). Microstructural features were investigated with scanning electron microscopy (SEM, FEI Quanta FEG 450), transmission electron microscopy (TEM, FEI TECNAI F30), and selected area electron diffraction (SAED).

To assess the hardness and toughness of the films, a Bruker TI−980 nanoindenter with a Berkovitch cone diamond tip was employed. Hardness measurements were performed by conducting six matrix indentations on the surface of each sample, spaced approximately 30 μm apart. The average hardness and elastic modulus were calculated using Oliver and Pharr's method based on load−displacement curves [22]. A penetration depth of 100 nm, less than 1/10 of the film thickness, was chosen to minimize substrate influence on the measurements, and drift rate was kept below 0.05. For toughness evaluation, a maximum load of 10 N was applied, and the penetration depth was set to be 4/5 of the film thickness to ensure visible cracking on the surface while reducing the effect of the substrate on the applied load.

3 Results

3.1 Structural evolution

Figure 2 shows the XRD patterns of VN/TiN−Ni nano-multilayered films with varying deposition time for the TiN−Ni modulation layer. The nano-multilayered films display the FCC structure of VN, with a clear preferential orientation towards the (200) plane, along with weaker peaks at the (111) and (220) planes. As the deposition time of the TiN−Ni modulation layer increases, the TiN−Ni sublayer grows in a stable FCC structure, influenced by the VN template layer, maintaining well-epitaxial growth that improves the crystalline integrity of the films. When the T_{TiN-Ni}:T_{VN} is 10:12, the diffraction peak for the (200) plane reaches its highest intensity, indicating optimized crystallinity of the films. At the same time, the full width at half maximum (FWHM) of the diffraction peak is minimized, reflecting the growth of larger grains. However, when the T_{TiN-Ni}:T_{VN} is 12:12, the XRD spectra become almost flat, and the intensity of the diffraction peaks decreases, suggesting that the films are in an amorphous state. Additionally, the TiN−Ni modulation layer phase is not detected, probably due to the shorter deposition time and lower sputtering power in RF mode.

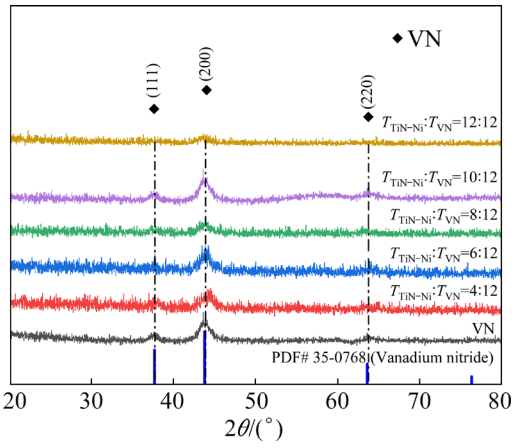

Fig. 2 XRD patterns of VN/TiN−Ni nano-multilayered films with different TiN−Ni deposition time

When T_{TiN-Ni}:T_{VN}=10:12, TiN−Ni modulation layer adopts the same crystal structure as the adjacent VN layer due to the template effect. The two sublayers maintain coherent epitaxial growth, resulting in the strongest diffraction peak intensity in

the XRD pattern. This coherent structure arises primarily from the lower interfacial energy during film deposition [8]. The thermodynamic incompatibility between TiN and Ni causes multiphase phenomena to emerge in the modulation layer, complicating its elemental composition. However, the specific distributions of TiN and Ni in the modulated layer remain challenging to characterize with current observational techniques due to the small thickness of the modulation layer.

The XPS spectra provide insight into the elemental composition of the sample surface. Figure 3 displays the spectra for V 2p, Ti 2p, Ni 2p, and N 1s of the VN/TiN−Ni nano-multilayered films with T_{TiN-Ni}:T_{VN} of 10:12. The V 2p band is split into two peaks, V $2p_{3/2}$ and V $2p_{1/2}$, separated by approximately 7.0 eV due to spin-orbit splitting, as shown in Fig. 3(b). The V $2p_{3/2}$ peak is located at 513.9 eV, which is attributed to V — N bonding [23,24]. In Fig. 3(c), the Ti 2p XPS peaks at 455.8 and 462.2 eV correspond to Ti—N and represent the spin-orbit splitting doublets of Ti $2p_{3/2}$ and Ti $2p_{1/2}$ [25,23]. In Fig. 3(d), the Ni 2p peaks at 853.7 and 871.5 eV correspond to Ni $2p_{3/2}$ and Ni $2p_{1/2}$ of Ni^0, while the peaks at 859.9 and 877.5 eV are satellite peaks, confirming the presence of metallic Ni in the modulation layer [26,27]. In Fig. 3(e), the N 1s spectrum shows a peak at 396.8 eV corresponding to VN. The Ti—N peak at 396.0 eV is not observed, probably due to the much lower Ti content in the nano-multilayered films compared to V [23,25]. The XPS results confirm that the VN/TiN−Ni nano-multilayered films consist of VN and TiN phases, and metallic Ni, and also indicate phase separation between TiN and Ni in the modulation layers.

The nanostructured composite films of TiN/Ni were previously investigated [28]. The findings revealed that Ni has the ability to fracture and split the TiN columnar grains into equiaxed nanocrystals, while forming a Ni interfacial phase that encapsulates the TiN nanocrystals. Once the Ni interfacial phase reaches a critical thickness, it tends to grow together with the adjacent TiN nanocrystals, reducing interfacial energy and thereby enhancing the crystallinity of the films [29,30].

Figure 4 shows the cross-sectional TEM images with SAED patterns of the nano-multilayered films when T_{TiN-Ni}:T_{VN}=10:12. In the medium-magnification image in Fig. 4(b), the nano-multilayered films clearly display a layered structure, with the dark and bright regions representing the VN and TiN−Ni sublayers, respectively. The high-

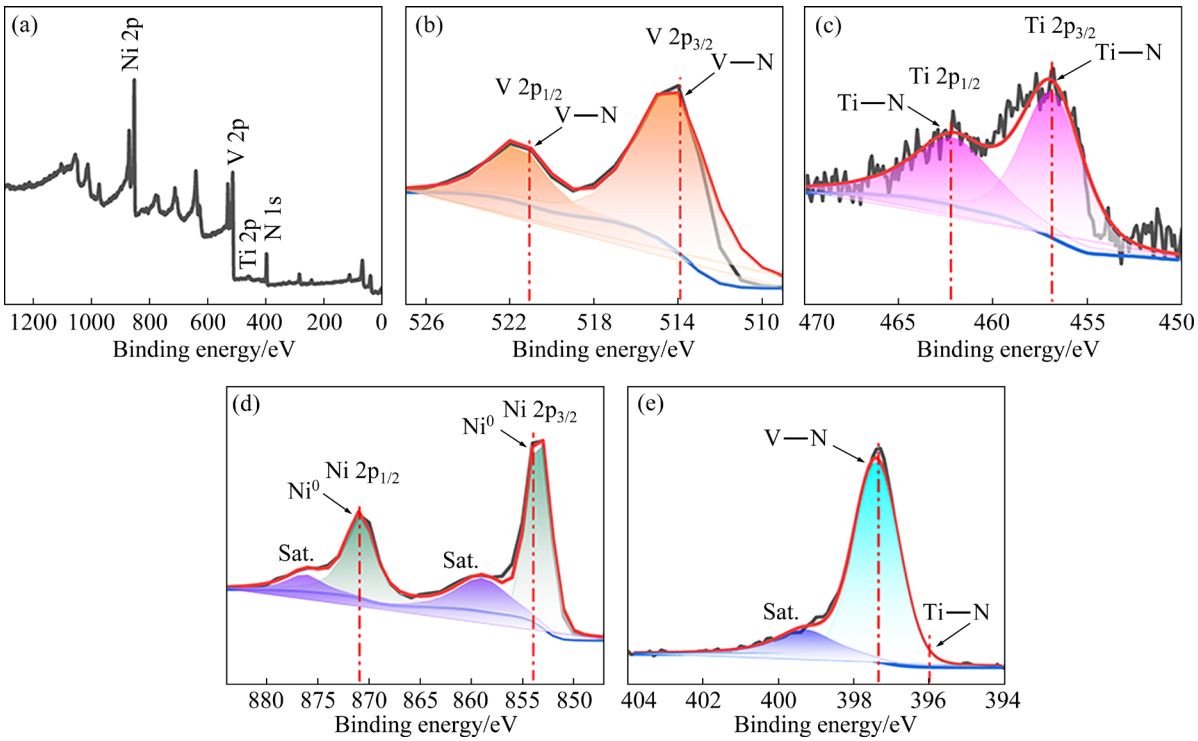

Fig. 3 (a) Survey XPS spectrum of VN/TiN−Ni nano-multilayered films with T_{TiN-Ni}:T_{VN} ratio of 10:12; (b) V 2p, (c) Ti 2p, (d) Ni 2p and (e) N 1s high-resolution XPS spectra

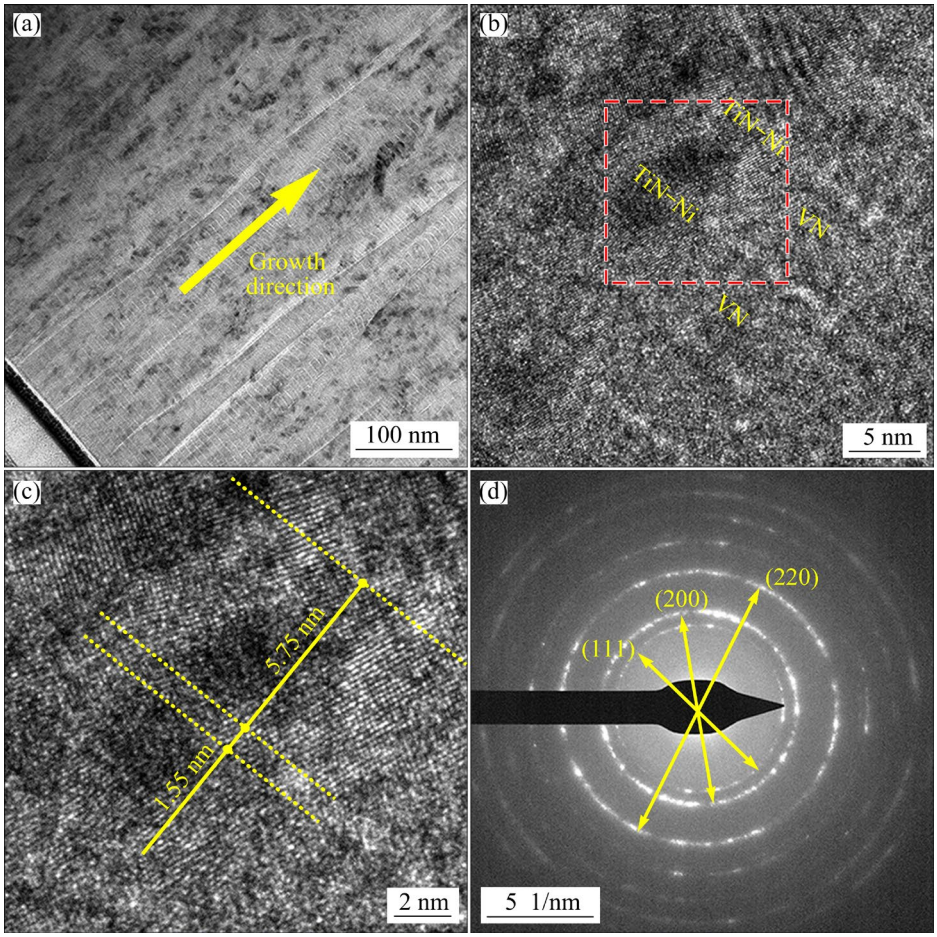

Fig. 4 Cross-sectional TEM images of VN/TiN−Ni nano-multilayered films with T_{TiN-Ni}:T_{VN} of 10:12 at (a) low-magnification, (b) medium-magnification, (c) high-magnification, respectively, and (d) SAED pattern in (b)

magnification image in Fig. 4(c) reveals an average modulation period of approximately 7.3 nm. Moreover, the lattice fringes extending through several sublayers and interfaces indicate the epitaxial growth of TiN−Ni grains on the VN sublayer, which gradually transitions into the FCC structure, forming a coherent interface with the VN template layer. This observation confirms the XRD results. The formation of the coherent interface in the VN/TiN−Ni nano-multilayered films is driven by the thermodynamic equilibrium between the coherent strain and interfacial energy, with the minimization of interfacial energy as the driving force. In Fig. 4(d), the continuous SAED rings show the (111), (200), and (220) orientations, further confirming the typical FCC structure observed in the XRD results.

Based on the above microstructural evolution, it can be inferred that the formation of coherent interfaces in VN/TiN−Ni nano-multilayered films, along with the phase separation of TiN and Ni in the modulation layers, will have a significant impact on the mechanical properties of the films.

Figure 5 presents the TEM−EDS analysis results of the VN/TiN−Ni nano-multilayered films with T_{TiN-Ni}:T_{VN} of 10:12. From the elemental composition in Fig. 5(a), it is observed that the concentrations of V and N are relatively high, while the concentrations of Ti and Ni are comparatively low. Along the deposition direction, the concentrations of V, Ti, and Ni exhibit a wave-like variation, with the V peaks corresponding to the troughs of Ti and Ni, while the N content remains relatively stable. In Fig. 5(b), the interfacial morphology shows that the V and N elements correspond to the template layer, while Ti and Ni are associated with the modulation layer. The depth profile in Fig. 5(b) reveals that the nano-multilayered films exhibit good homogeneity and stability. The VN and TiN−Ni sublayers are well aligned, with clearly defined interfaces and sharp contrast, forming a well-structured nano-multilayer, consistent with the TEM cross-sectional image in

Fig. 4. The average thicknesses of the VN template layer and TiN−Ni modulation layer in the VN/TiN−Ni nano-multilayered films are (5.75±0.25) and (1.55±0.23) nm, respectively, for T_{TiN-Ni}:T_{VN} of 10:12.

As shown in Fig. 6, the cross-sectional SEM images of both the VN monolithic film and VN/TiN−Ni nano-multilayered films display uniform film thickness, smooth surfaces, and no apparent defects. In Figs. 6(b−e), as the deposition time of the TiN−Ni layer increases, the cross-section of the nano-multilayered films reveals numerous columnar grains. When T_{TiN-Ni}:T_{VN}=10:12, as seen in Fig. 6(e), transverse stripes become visible, indicating the presence of a nano-multilayered structure. With further increases in the TiN−Ni deposition time, when T_{TiN-Ni}:T_{VN}=12:12, the columnar grain structure disappears, and the nano-

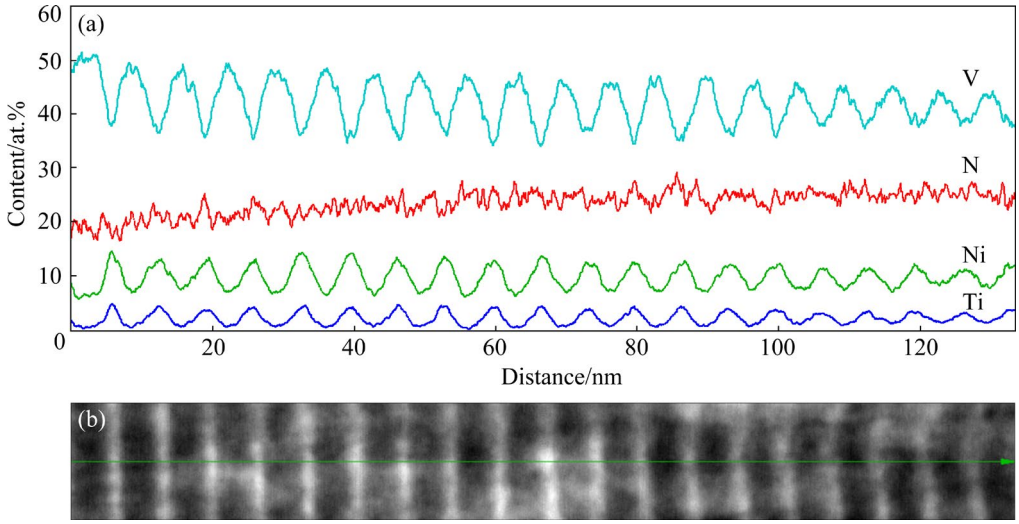

Fig. 5 TEM−EDS analysis of VN/TiN−Ni nano-multilayered films with T_{TiN-Ni}:T_{VN} of 10:12: (a) Elemental composition; (b) Elemental depth profile with corresponding part of TEM cross-section image

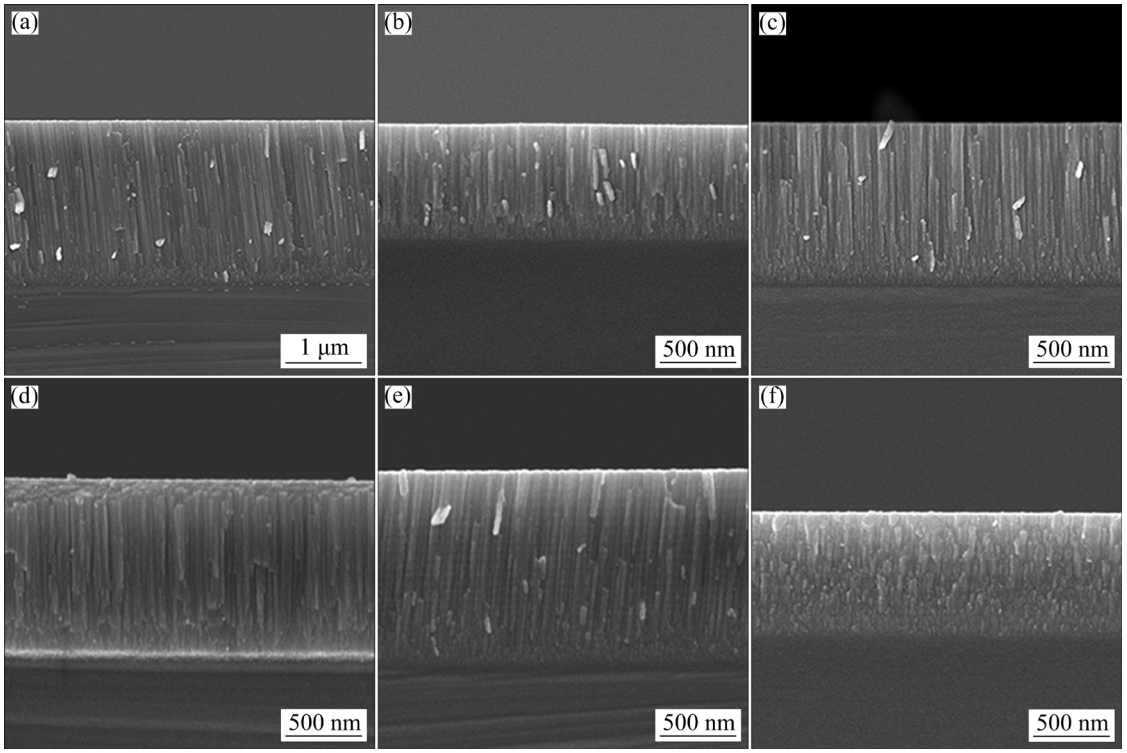

Fig. 6 Cross-sectional SEM images of VN/TiN−Ni nano-multilayered films with different deposition time: (a) VN monolithic film; (b) T_{TiN-Ni}:T_{VN}=4:12; (c) T_{TiN-Ni}:T_{VN}=6:12; (d) T_{TiN-Ni}:T_{VN}=8:12; (e) T_{TiN-Ni}:T_{VN}=10:12; (f) T_{TiN-Ni}:T_{VN}=12:12

multilayered film transitions into amorphous state, as shown in Fig. 6(f). The thickness of the nano-multilayered films initially increases and then decreases with increasing deposition time of the TiN−Ni layer, measuring 750, 1063, 1166, 1241, and 782 nm, respectively. The thickness reaches its maximum when T_{TiN-Ni}:T_{VN}=10:12. Differences in microstructures lead to variations in nucleation and crystallization rates during deposition, ultimately influencing the deposition thickness of the nano-multilayered films [31,32].

3.2 Hardness and elastic modulus

Under identical preparation conditions, the hardness and elastic modulus of the VN monolithic film and the VN/TiN−Ni nano-multilayered films are compared in Fig. 7. The VN monolithic film exhibits values of 18.2 GPa and 204.1 GPa, respectively. For the VN/TiN−Ni nano-multilayered films, these properties initially increase and then decrease as the T_{TiN-Ni}:T_{VN} ratio rises. The peak values, 23.9 GPa and 317 GPa, occur at T_{TiN-Ni}:T_{VN} of 10:12. However, as the ratio reaches 12:12, these values drop to 18.7 GPa and 207.9 GPa, respectively. This decline is attributed to the amorphous state of the nano-multilayered films when the TiN−Ni modulation layer becomes thicker, leading to a disruption of the coherent interfacial structure.

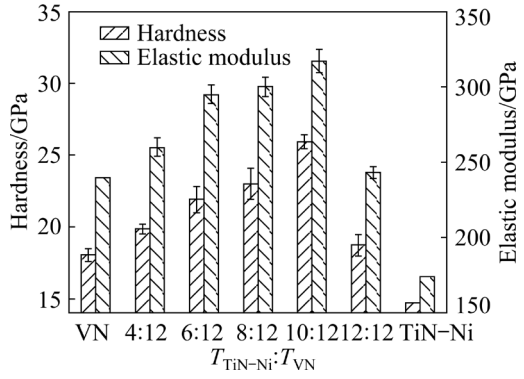

Fig. 7 Hardness and elastic modulus for VN/TiN−Ni nano-multilayered films with different TiN−Ni deposition time

3.3 Toughness

Material toughness can be evaluated using H^3/E^2 and H/E [33−36]. Here, H^3/E^2 reflects the plastic deformability of the films, where higher values indicate an enhanced ability to absorb energy during deformation and fracture. Meanwhile, H/E measures the resistance of the films to cracking, with larger values suggesting superior wear resistance.

Figure 8 illustrates the H/E and H^3/E^2 values for both the VN monolithic film and VN/TiN−Ni nano-multilayered films. The VN monolithic film exhibits values of 0.075 and 0.102 GPa, respectively. Notably, the nano-multilayered films display higher values than the monolithic film, showing an initial increase followed by a decrease as the T_{TiN-Ni}:T_{VN} ratio increases, similar to the trend observed for hardness. At T_{TiN-Ni}:T_{VN} of 10:12, the peak values of 0.082 and 0.173 GPa are achieved, indicating optimal toughness. However, when the ratio reaches 12:12, the values decrease to 0.077 and 0.111 GPa, signifying a deterioration in the toughness of the films.

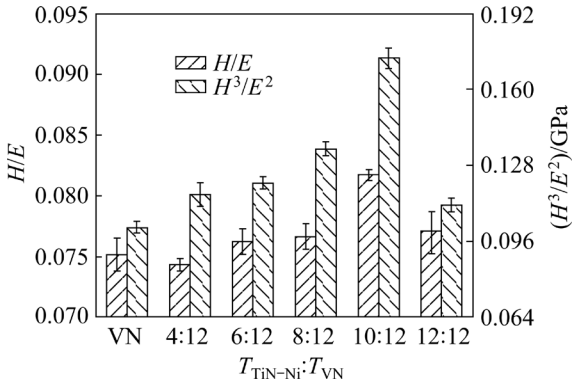

Fig. 8 H/E and H^3/E^2 ratios of VN/TiN−Ni nano-multilayered films with different TiN−Ni deposition time

Figure 9 compares the nanoindentation crack lengths, c, of the VN monolithic film and the VN/TiN−Ni nano-multilayered films. The crack length (c) is measured nine times, with the maximum and minimum values excluded, and the mean and standard deviation calculated from the remaining seven measurements. Under the same loading conditions, the monolithic film exhibit a c value of 11.1 μm, as shown in Fig. 9(a). In contrast, the nano-multilayered films display an initial reduction in c value, followed by a gradual increase. Despite this variation, all c values remain smaller than the value of the monolithic film, indicating that the nano-multilayered structure enhances toughness compared to the monolithic film. As depicted in Fig. 9(c), the shortest c value, 5.9 μm, occurs when the T_{TiN-Ni}:T_{VN} is 6:12, signifying the highest fracture toughness among the nano-multilayered films. However, with an increase in TiN−Ni sublayer deposition time (T_{TiN-Ni}:T_{VN} of 12:12), the indentation morphology

becomes irregular. This leads to a decline in fracture toughness, as illustrated in Fig. 9(f).

Figure 10 presents FIB-milled cross-sectional TEM images of the nanoindentation deformation zone in the VN/TiN−Ni nano-multilayered films with a T_{TiN-Ni}:T_{VN} of 10:12. Cracks initiate at the surface and propagate into the interior of the films. Both radial and lateral cracks are visible on either side of the nanoindentation, as illustrated in Fig. 10(c). An enlarged view of the crack-tip region,

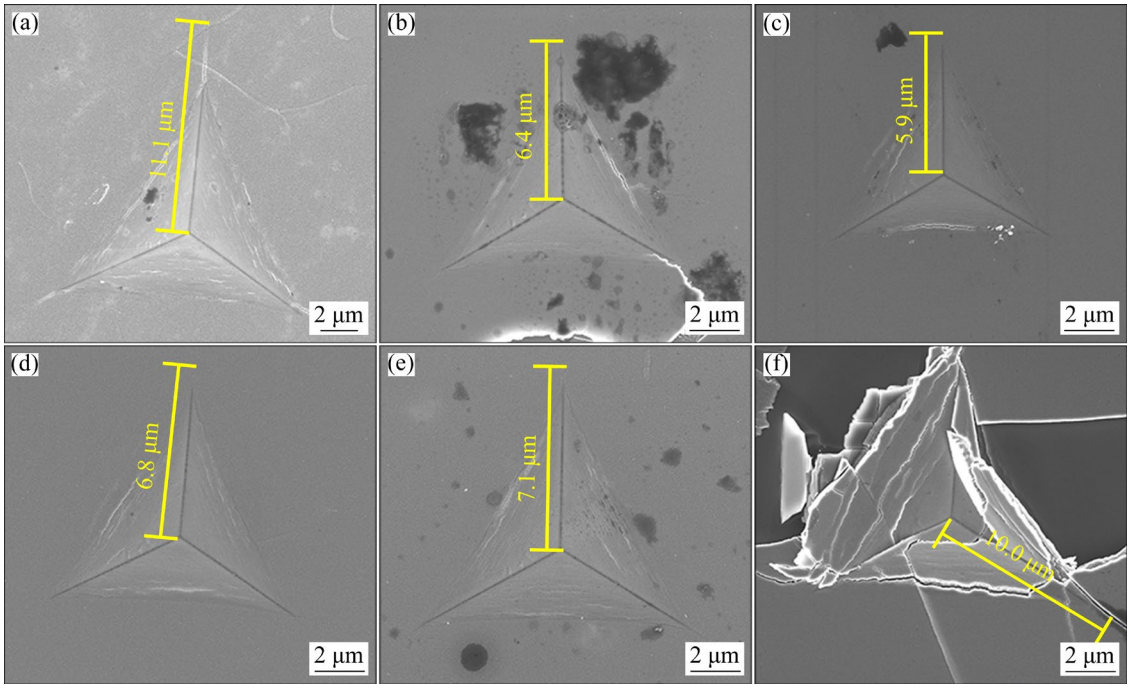

Fig. 9 SEM images of indentation-induced cracking for VN/TiN−Ni nano-multilayered films with different TiN−Ni deposition time: (a) VN monolithic film; (b) T_{TiN-Ni}:T_{VN}=4:12; (c) T_{TiN-Ni}:T_{VN}=6:12; (d) T_{TiN-Ni}:T_{VN}=8:12; (e) T_{TiN-Ni}:T_{VN}=10:12; (f) T_{TiN-Ni}:T_{VN}=12:12

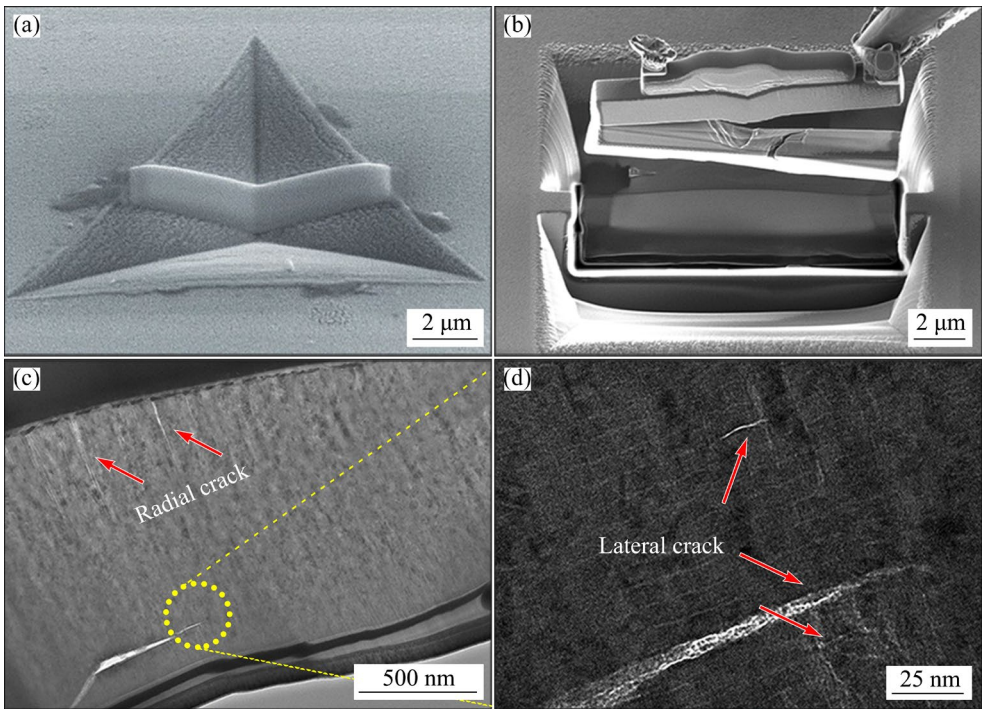

Fig. 10 Crack-tip cross-sectional TEM images of VN/TiN−Ni nano-multilayered films with T_{TiN-Ni}:T_{VN} of 10:12: (a) FIB-milling position; (b) In low-magnification; (c) In medium-magnification; (d) In high-magnification

shown in Fig. 10(d), reveals distinct lateral cracks at the interfaces between the VN and TiN−Ni layers. These cracks propagate under residual stress [37]. Crack deflection at the interfaces reduces the crack-driving force, contributing to film toughening and enhancing its damage resistance [38].

4 Discussion

4.1 Microstructure evolution

Based on XRD and TEM results, when the T_{TiN-Ni}:T_{VN} is no greater than 10:12, the TiN−Ni layer undergoes a transformation into an FCC structure. This occurs due to the "template effect" of the VN layer, enabling coherent growth between the TiN−Ni and VN layers. In the VN/TiN−Ni nano-multilayered films, the TiN−Ni crystal layer further enhances the growth and structural integrity of the VN crystal layer, as evidenced by intensified diffraction peaks in the XRD patterns. A similar mechanism is observed in other nano-multilayered films, such as TiN/AlTiN [39], Ti/TiN [40,41], Cu/TiN [42], and TiBN/TiN [43]. The structural transformation caused by the TiN−Ni modulation layer in VN/TiN−Ni nano-multilayered films can be explained using a thermodynamic model [44]:

$$E_{total}=(E_{bulk}+E_{str})t_{TiN-Ni}+E_{int} \quad (1)$$

The total energy of the TiN−Ni layer (E_{total}) comprises three components: the strain-free bulk energy (E_{bulk}), strain energy (E_{str}), and interfacial energy (E_{int}). The thickness of the TiN−Ni modulation layer (t_{TiN-Ni}) significantly influences the energy balance, with E_{int} representing the interfacial energy between the VN and TiN−Ni layers. When T_{TiN-Ni}:T_{VN} is below 10:12, the TiN−Ni layer is thin enough that E_{int} becomes the dominant factor in E_{total}, allowing epitaxial growth between the TiN−Ni and VN layers. However, as the ratio increases to 12:12, t_{TiN-Ni} surpasses a critical threshold. At this point, E_{bulk} and E_{str} contribute more significantly to E_{total}, disrupting the coherent interface structure between the VN and TiN−Ni layers.

The microstructural evolution of VN/TiN−Ni nano-multilayered films is illustrated in Fig. 11. When the T_{TiN-Ni}:T_{VN} is less than 10:12, the TiN−Ni composite layer undergoes a structural transformation driven by the template effect of the VN layer. This process establishes a coherent interface between the VN and TiN−Ni layers, significantly lowering the interfacial energy between them.

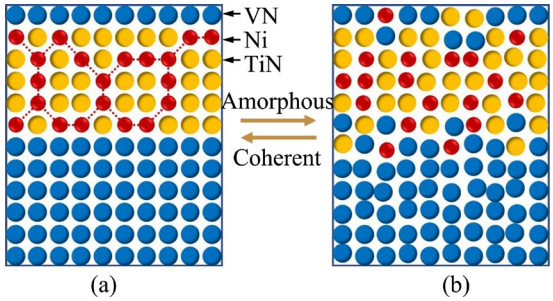

Fig. 11 Schematic of microstructural evolution of VN/TiN−Ni nano-multilayered films with different TiN−Ni deposition time: (a) T_{TiN-Ni}:T_{VN}=10:12; (b) T_{TiN-Ni}:T_{VN}=12:12

Due to the thermodynamic incompatibility between Ni and TiN, the Ni phase separates from the TiN−Ni composite structure, forming an interfacial phase that encases the TiN nanograins to minimize interfacial energy [29], as indicated by the dashed line in Fig. 11(a). The epitaxial relationship between the Ni interface and the TiN grains promotes the crystallinity in the films. The combination of the coherent interface and the phase-separation interface within the modulation layer helps to suppress dislocation motion, thereby enhancing the strengthening effect of the nano-multilayered films.

When the T_{TiN-Ni}:T_{VN} reaches 12:12, the coherent growth structure between the VN and TiN−Ni layers is no longer sustained, and the template effect of the VN layer on the TiN−Ni layer diminishes, as shown in Fig. 11(b). Consequently, the crystallinity of the films deteriorates, and the cross-sectional morphology exhibits an amorphous state, as seen in Fig. 6(f). This microstructural evolution results in the loss of the strengthening effect, leading to a rapid decline in the mechanical properties of the films.

4.2 Strengthening and toughening mechanisms

The strengthening effect of VN/TiN−Ni nano-multilayered films can be explained using the Koehler modulus-difference theory [45], alternating stress-field strengthening [46], and the Hall−Petch relationship [47]. According to the Koehler modulus-difference theory, dislocations crossing the

film interface are resisted by the two sublayers due to their differing shear moduli. A greater modulus difference increases this resistance, enhancing the strengthening effect of the films. In this study, the shear moduli of VN and TiN−Ni monolithic films are 19.3 GPa and 14.8 GPa, respectively, and the modulus difference between adjacent sublayers increases at a higher T_{TiN-Ni}:T_{VN} ratio. It is important to note that the formation of coherent interfaces is a critical condition for the applicability of the modulus-difference theory [28].

The theoretical lattice parameters for VN, TiN, and Ni are 4.12, 4.241, and 3.52 Å, respectively. Although VN and TiN−Ni share the same crystal structure, the lower-content TiN and the Ni interface, with their smaller lattice parameters, are subjected to tensile stresses. In contrast, VN, with its larger lattice parameters, undergoes compressive stresses within the epitaxial growth structure. This interplay results in an alternating compressive−tensile stress field along the growth direction, which hinders the dislocation motion and significantly enhances the strengthening of the VN/TiN−Ni nano-multilayered films. Additionally, the insertion of modulation layers disrupts the formation of coarse columnar grains, leading to grain refinement that further increases the strength of the films.

The critical stress intensity factor, K_{IC}, is used to assess the fracture toughness of film materials and is defined by Eq. (2) [48]:

$$K_{IC} = \delta\left(\frac{E}{H}\right)^{1/2}\left(\frac{P}{c^{3/2}}\right) \quad (2)$$

where δ is assigned a value of 0.016 for a Berkovich-type indenter, P is the maximum load (mN), and c represents the average radial crack length (μm).

The K_{IC} values for the VN monolithic film and the VN/TiN−Ni nano-multilayered films are shown in Fig. 12. The VN monolithic film has a K_{IC} value of 1.24 MPa·m$^{1/2}$. As the TiN−Ni layer deposition time increases, the K_{IC} values of the nano-multilayered films initially rise and then fall. The peak K_{IC} value of 1.86 MPa·m$^{1/2}$ occurs at T_{TiN-Ni}:T_{VN} of 10:12. However, as the T_{TiN-Ni}:T_{VN} ratio increases further to 12:12, the K_{IC} value decreases to 1.17 MPa·m$^{1/2}$. The fracture toughness of the VN/TiN−Ni nano-multilayered films is roughly 50% higher than that of the VN monolithic film.

Multilayered structure is an effective strategy for enhancing the hardness and toughness of films [49,50]. The toughening mechanisms in VN/TiN−Ni nano-multilayered films include beneficial coherent interfaces and phase separation in the TiN−Ni layers. The nano-multilayered interface helps to limit shear cracking by facilitating interlayer slip, acting as an additional stress-relief mechanism [51]. At the same time, the coherent interface between the VN and TiN−Ni layers enables the alternating stress field to lower the activation energy needed for dislocation movement, thereby improving fracture toughness [52]. When cracks propagate along the interface, the interlayer can directly cause crack deflection, hindering crack growth and greatly enhancing the fracture resistance of the films. The greater the crack deflection along the interface, the more effectively the loading stress is released, resulting in a more pronounced toughening effect.

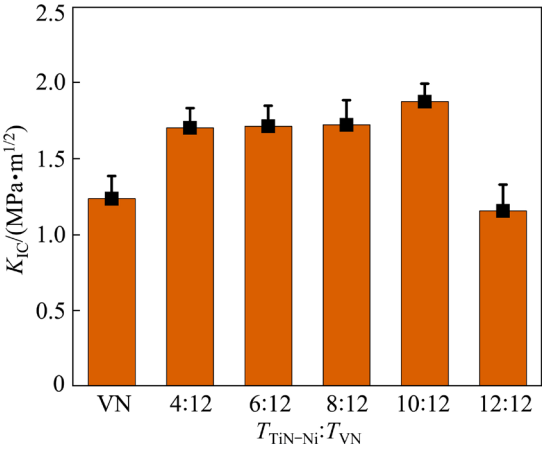

Fig. 12 Fracture toughness of VN/TiN−Ni nano-multilayered films with different TiN−Ni deposition time

In nanocomposite structures, metals like Ni, Cu, or Y typically do not form stable nitrides and instead exist as separate interfacial phases [53−55]. The TiN−Ni nanocomposite films have been previously developed [29]. When the Ni ratio is below 4:21, the thermodynamic incompatibility between TiN and Ni causes the Ni interface phase to coherently grow with the adjacent TiN nanocrystals. This growth reduces interfacial energy and improves the crystallinity of the films. Moreover, the inclusion of Ni disrupts and subdivides the TiN columnar grains into equiaxed TiN nanocrystals, leading to a continuous decrease in grain size, enhanced film hardness, and improved toughness [28]. When

T_{TiN-Ni}:T_{VN} is 10:12, the separate TiN and Ni layers within the modulation layer adopt an FCC structure, influenced by the template effect of the VN layer. Simultaneously, the coherent structure within the modulation layer positively affects the mechanical properties of the films, effectively hindering the initiation and propagation of cracks.

As a result, the VN/TiN−Ni nano-multilayered films exhibit superior fracture toughness compared to monolithic VN films. Similar effects in enhancing fracture toughness have been observed in Fe-doped Cr(Fe)/CrN composite materials [56], Ni-enhanced TiB_2 coatings [57], W-doped Ni/Ni_3Al−W films [58], and Ni mixed with nc-CrAlN/*a*-SiN_x films [59]. These findings suggest that the presence of an appropriate amount of a metal-ductile phase contributes positively to the toughening effect of multilayer films.

5 Conclusions

(1) When T_{TiN-Ni}:T_{VN}=10:12, the diffraction peak intensities of the VN/TiN−Ni nano-multilayered films reach their maximum, resulting in optimized crystallinity. The films are composed of VN, TiN, and Ni phases.

(2) The hardness and elastic modulus achieve peak values of 25.9 GPa and 317 GPa, respectively, with H/E and H^3/E^2 values of 0.082 and 0.173 GPa, when the T_{TiN-Ni}:T_{VN} ratio is 10:12. The optimal K_{IC} value is 1.88 MPa·$m^{1/2}$, which represents an improvement of approximately 50% compared to the VN monolithic film.

(3) The strengthening of VN/TiN−Ni nano-multilayered films is primarily attributed to the modulus difference theory, the alternating stress field, and the Hall−Petch relationship at coherent interface. Additionally, the favorable coherent interfacial structure and the formation of separated phases within the modulation layer contribute to the enhanced fracture toughness of the nano-multilayered films.

CRediT authorship contribution statement

Wen-jie CHENG: Experimental, Analysis, Writing – Original draft, Writing – Review & editing, Funding acquisition; **Ping LIU:** Analysis, Writing – Review & editing; **Xin-fa ZHU:** Analysis, Writing – Review & editing; **Yi MENG:** Analysis, Writing – Review & editing; **Hong-mei LU:** Analysis, Writing – Review & editing; **Peter K. LIAW:** Analysis, Writing – Review & editing, Supervision; **Wei LI:** Analysis, Writing – Review & editing, Supervision, Funding acquisition.

Declaration of competing interest

The authors declare that they have no known competing financial interests or personal relationships that could have appeared to influence the work reported in this paper.

Acknowledgments

The present research was financially supported by the National Natural Science Foundation of China (No. 51971148), the Key Project Foundation of Hanjiang Normal University, China (No. XJ2024A09), the Excellent Young and Middle-aged Science and Technology Innovation Team Project in Higher Education Institutions of Hubei Province, China (No. T2020024), and the Shanghai Engineering Research Center of High-Performance Medical Device Materials, China (No. 20DZ2255500).

References

[1] AISSANI L, ALHUSSEIN A, NOUVEAU C, GHELANI L, ZAABAT M. Influence of film thickness and Ar−N_2 plasma gas on the structure and performance of sputtered vanadium nitride coatings [J]. Surface & Coatings Technology, 2019, 378: 124948.

[2] XIAN G, XIONG J, FAN H Y, JIANG F, ZHAO H B, XIAN L J, QIN Z H. Mechanical and wear properties of TiN films on differently pretreated TiCN-based cermets [J]. Applied Surface Science, 2021, 570: 151180.

[3] JALALI B M, OMIDVAR H, ZAMANIAN A, AGHAZADEH M J, JALALI H. Characterization, wear behavior and biocompatibility of HA/Ti composite and functionally graded coatings deposited on Ti−6Al−4V substrate by mechanical coating technique [J]. Transactions of Nonferrous Metals Society of China, 2024, 34(2): 547−559.

[4] MEI Z G, BHATTACHARYA S, YACOUT A M. First-principles study of fracture toughness enhancement in transition metal nitrides [J]. Surface & Coatings Technology, 2019, 357: 903−909.

[5] KINDLUND H, SANGIOVANNI D G, PETROV I, GREENE J E, HULTMAN L. A review of the intrinsic ductility and toughness of hard transition-metal nitride alloy thin films [J]. Thin Solid Films, 2019, 688: 137479.

[6] GAO Z, BUCHINGER J, KOUTNÁ N, WOJCIK T, HAHN R, MAYRHOFER P H. Ab initio supported development of TiN/MoN superlattice thin films with improved hardness and toughness [J]. Acta Materialia, 2022, 231: 117871.

[7] SANGIOVANNI D G. Inherent toughness and fracture mechanisms of refractory transition-metal nitrides via density-functional molecular dynamics [J]. Acta Materialia, 2018, 151: 11−20.

[8] BUCHINGER J L, KOUTNÁ N, CHEN Z, ZHANG Z L, MAYRHOFER P H, HOLEC D, BARTOSIK M. Toughness enhancement in TiN/WN superlattice thin films [J]. Acta Materialia, 2019, 172: 18−29.

[9] BELTRAMI M, MAVRIČ A, ZILIO S D, FANETTI M, KAPUN G, LAZZARINO M, SBAIZERO O, ČEKADA M. A comparative study of nanolaminate CrN/Mo_2N and CrN/W_2N as hard and corrosion resistant coatings [J]. Surface & Coatings Technology, 2023, 455: 129209.

[10] CHEN X, TANG Z. Ultra-high thermal conductivity FGN/PVA/MXene composite films with good electrical insulation [J]. Composites Science and Technology, 2023, 242: 110208.

[11] IZADINIA M, SOLTANI R, HEYDARZADEH S M, MOSTAGHIMI J. Thermal insulation capability and adhesion strength of unpyrolyzed thick thermal barrier coatings [J]. Transactions of Nonferrous Metals Society of China, 2024, 34(4): 1226−1236.

[12] LIU Y M, TIAN L, CHANG J X, AN M R, PEI Z L, FAN D. Effect of modulation ratio on structure and mechanical properties of WB_2/CrN films deposited by direct-current magnetron sputtering [J]. Journal of Alloys and Compounds, 2021, 851: 156852.

[13] PAN Y P, DONG L, LIU N, YU J G, LI C, LI D J. Investigating the influence of epitaxial modulation on the evolution of superhardness of the VN/TiB_2 multilayers [J]. Applied Surface Science, 2016, 390: 406−411.

[14] FU T, ZHANG Z J, PENG X H, WENG S Y, MIAO Y H, ZHAO Y B, FU S Y, HU N. Effects of modulation periods on mechanical properties of V/VN nano-multilayers [J]. Ceramics International, 2019, 45(8): 10295−10303.

[15] WANG R, LI H Q, LI R S, MEI H J, ZOU C W, ZHANG T F, WANG Q M, KIM K H. Thermostability, oxidation, and high-temperature tribological properties of nano-multilayered AlCrSiN/VN coatings [J]. Ceramics International, 2022, 48(9): 11915−11923.

[16] ZHOU T, CHEN H, YUE Y N, FANG X Y, ZHANG R Q, GAO X, CAI Z B. Effect of coating thickness on interfacial adhesion and mechanical properties of Cr-coated zircaloy [J]. Transactions of Nonferrous Metals Society of China, 2023, 33(9): 2672−2686.

[17] LIU W, SHEN Q, YANG M, GAO T, JI B, TU R, ZHANG S. High hardness and toughness potential TiN/TiSiN gradient nano-multilayer coating structure by finite element study [J]. Ceramics International, 2024, 50(6): 9034−9046.

[18] LI J, TAN C, LUO X, XIE Z, ZHONG X, WANG J, SONG H. Preparation and toughness optimization of (AlCrSiN/TiN)20/Ti multilayer multiscale bionic tool coatings [J]. Applied Surface Science, 2023, 634: 157585.

[19] DU J W, CHEN L, ZHANG J, XU Y X, LIU Z R, PEI F. Tuning mechanical properties of TiAlSiN/TiAlN multilayers by interfacial structure [J]. Materials Characterization, 2024, 210: 1−6.

[20] LORENTZON M, MEINDLHUMER M, PALISAITIS J, GRECZYNSKI G, KECKES J, ROSEN J, HULTMAN L, BIRCH J, GHAFOOR N. Toughness enhancement in TiN/$Zr_{0.37}Al_{0.63}N_{1.09}$ multilayer films [J]. Acta Materialia, 2024, 273: 119979.

[21] ZHOU C, WANG J J, MENG J, LI W, LIU P, ZHANG K, MA F C, MA X, FENG R, LIAW P K. Effects of modulation layer thickness on fracture toughness of a TiN/AlN−Ni multilayer film [J]. Materials & Design, 2022, 222: 111097.

[22] OLIVER W C, PHARR G M. An improved technique for determining hardness and elastic modulus using load and displacement sensing indentation experiments [J]. Journal of Materials Research, 1992, 7(6): 1564−1583.

[23] LIU P, WEI Y N, CUI S, WEI H Y, BU J L, NI J, LV D F, CUI Y. Fabrication of mesoporous TiVN powders and their electrochemical performance [J]. Journal of the Ceramic Society of Japan, 2019, 127(10): 728−735.

[24] LI S Q, SUN X, YAO Z H, ZHONG X, CAO Y Y, LIANG Y L, WEI Z Z, DENG S W, ZHUANG G L, LI X N, WANG J G. Biomass valorization via paired electrosynthesis over vanadium nitride-based electrocatalysts [J]. Advanced Functional Materials, 2019, 29(42): 1904780.

[25] GRECZYNSKI G, MRÁZ S, HULTMAN L, SCHNEIDER J M. Venting temperature determines surface chemistry of magnetron sputtered TiN films [J]. Applied Physics Letters, 2016, 108(4): 041603.

[26] FAN L, LIU P F, YAN X, GU L, YANG Z Z, YANG H G, QIU S, YAO X. Atomically isolated nickel species anchored on graphitized carbon for efficient hydrogen evolution electrocatalysis [J]. Nature Communications, 2016, 7: 1−7.

[27] HUANG H, ZHAO Y, BAI Y M, LI F M, ZHANG Y, CHEN Y. Conductive metal−organic frameworks with extra metallic sites as an efficient electrocatalyst for the hydrogen evolution reaction [J]. Advanced Science, 2020, 7(9): 1−9.

[28] LI W, LIU P, ZHAO S, ZHANG K, MA F, LIU X, CHEN X, HE D. Microstructural evolution, mechanical properties and strengthening mechanism of TiN/Ni nanocomposite film [J]. Journal of Alloys and Compounds, 2017, 691: 159−164.

[29] LI W, LIU P, ZHU X D, PAN D, ZHANG K, MA F C, LIU X K. Effect of Si content on microstructural evolution and superhardness effect of TiN/CrAlSiN nanomultilayered films [J]. Journal of Alloys and Compounds, 2015, 650: 592−597.

[30] KIM I W, LI Q, MARKS L D, BARNETT S A. Critical thickness for transformation of epitaxially stabilized cubic AlN in superlattices [J]. Applied Physics Letters, 2001, 78(7): 892−894.

[31] KHOO C Y, LIU H, SASANGKA W A, MADE R I, TAMURA N, KUNZ M, BUDIMAN A S, GAN C L, THOMPSON C V. Impact of deposition conditions on the crystallization kinetics of amorphous GeTe films [J]. Journal of Materials Science, 2016, 51(4): 1864−1872.

[32] VOUTSAS A T, HATALIS M K, BOYCE J, CHIANG A. Raman spectroscopy of amorphous and microcrystalline silicon films deposited by low-pressure chemical vapor deposition [J]. Journal of Applied Physics, 1995, 78(12): 6999−7006.

[33] PSHYK A V, COY L E, NOWACZYK G, KEMPIŃSKI M, PEPLIŃSKA B, POGREBNJAK A D, BERESNEV V M, JURGA S. High temperature behavior of functional TiAlBSiN nanocomposite coatings [J]. Surface & Coatings Technology, 2016, 305: 49−61.

[34] REN P, ZHANG K, WEN M, DU S X, CHEN J H, ZHENG W T. The roles of Ag layers in regulating strengthening-toughening behavior and tribochemistry of the Ag/TaC nano-multilayer films [J]. Applied Surface Science, 2018, 445: 415−423.

[35] KONG Y, TIAN X B, GONG C Z, CHU P K. Enhancement of toughness and wear resistance by CrN/CrCN multilayered coatings for wood processing [J]. Surface & Coatings Technology, 2018, 344: 204−213.

[36] KRAVCHENKO Y O, COY E, PEPLIŃSKA B, IATSUNSKYI I, ZAŁĘSKI K, KEMPIŃSKI M, BERESNEV V M, PSHYK A V, POGREBNJAK A D. Micro-mechanical investigation of $(Al_{50}Ti_{50})N$ coatings enhanced by ZrN layers in the nanolaminate architecture [J]. Applied Surface Science, 2020, 534: 147573.

[37] HAGAN J T, SWAIN M V. The origin of median and lateral cracks around plastic indents in brittle materials [J]. Journal Physics D: Applied Physics, 1978, 11(15): 2091−2102.

[38] HE M Y, HUTCHINSON J W. Crack deflection at an interface between dissimilar elastic materials [J]. International Journal of Solids and Structures, 1989, 25(9): 1053−1067.

[39] SURESHA S J, MATH S, JAYARAM V, BISWAS S K. Toughening through multilayering in TiN−AlTiN films [J]. Philosophical Magazine, 2007, 87(17): 2521−2539.

[40] ZHAO C L, ZHU Y B, YUAN Z W, LI J L. Structure and tribocorrosion behavior of Ti/TiN multilayer coatings in simulated body fluid by arc ion plating [J]. Surface & Coatings Technology, 2020, 403: 126399.

[41] MISHRA A K, GOPALAN H, HANS M, KIRCHLECHNER C, SCHNEIDER J M, DEHM G, JAYA B N. Strategies for damage tolerance enhancement in metal/ceramic thin films: Lessons learned from Ti/TiN [J]. Acta Materialia, 2022, 228: 117777.

[42] MIRAZ A S M, MENG W J, RAMACHANDRAN B R, WICK C D. Computational observation of the strengthening of Cu/TiN metal/ceramic interfaces by sub-nanometer interlayers and dopants [J]. Applied Surface Science, 2021, 554: 149562.

[43] ZHOU S Y, PELENOVICH V O, HAN B, YOUSAF M I, YAN S J, TIAN C X, FU D J. Effects of modulation period on microstructure, mechanical properties of TiBN/TiN nanomultilayered films deposited by multi arc ion plating [J]. Vacuum, 2016, 126: 34−40.

[44] LI W, LIU P, ZHANG K, MA F C, LIU X K, CHEN X H, HE D H. Structural evolution of yttrium nanolayer inserted in FeNi/Y nanomultilayered film [J]. Applied Surface Science, 2014, 317: 935−939.

[45] KOEHLER J S. Attempt to design a strong solid [J]. Physical Review B, 1970, 2(2): 547−551.

[46] LI G Y, HAN Z H, TIAN J W, XU J H, GU M Y. Alternating stress field and superhardness effect in TiN/NbN superlattice films [J]. Journal of Vacuum Science & Technology A, 2002, 20(3): 674−677.

[47] ANDERSON P M, LI C. Hall-Petch relations for multilayered materials [J]. Nanostructured Materials, 1995, 5(3): 349−362.

[48] LAWN B R, EVANS A G, MARSHALL D B. Elastic/plastic indentation damage in ceramics: The median/radial crack system [J]. Journal of the American Ceramic Society, 1980, 63(9/10): 574−581.

[49] SCHLO M, KIRCHLECHNER C, PAULITSCH J, KECKES J, MAYRHOFER P H. Effects of structure and interfaces on fracture toughness of CrN/AlN multilayer coatings [J]. Scripta Materialia, 2013, 68: 917−920.

[50] WANG S, XIE M Y, HUANG H B, KANG M, LIU R, CHEN C, ZHANG Z, ZHONG Z H, WU Y C. Diffusion behavior and bending fracture mechanism of W/Ti multilayer composites [J]. Journal of Alloys and Compounds, 2021, 879: 160451.

[51] VERMA N, CADAMBI S, JAYARAM V, BISWAS S K. Micromechanisms of damage nucleation during contact deformation of columnar multilayer nitride coatings [J]. Acta Materialia, 2012, 60: 3063−3073.

[52] WANG C, PUREZA J M, YANG Y Q, CHUNG Y W. Investigation of hardness and fracture toughness properties of Fe/VC multilayer coatings with coherent interfaces [J]. Surface & Coatings Technology, 2016, 288: 179−184.

[53] ŠŮNA J, MUSIL J, ONDOK V, HAN J G. Enhanced hardness in sputtered Zr−Ni−N films [J]. Surface & Coatings Technology, 2006, 200: 6293−6297.

[54] MUSIL J, POLÁKOVÁ H. Hard nanocomposite Zr−Y−N coatings, correlation between hardness and structure [J]. Surface & Coatings Technology, 2000, 127: 99−106.

[55] MUSIL J, HRUBÝ H, ZEMAN P, ZEMAN H, ČERSTVÝ R, MAYRHOFER P H, MITTERER C. Hard and superhard nanocomposite Al−Cu−N films prepared by magnetron sputtering [J]. Surface & Coatings Technology, 2001, 142/143/144: 603−609.

[56] HE J, LAN X, WAN J, LIU H, LIU Z, JIAO D. Modifying Cr/CrN composite structure by Fe addition: Toward manufacturing cost-effective and tough hard coatings [J]. Applied Surface Science, 2021, 545: 149025−149032.

[57] WANG H Y, WANG B, LI S Z, XUE Q J, HUANG F. Toughening magnetron sputtered TiB_2 coatings by Ni addition [J]. Surface & Coatings Technology, 2013, 232: 767−774.

[58] ZHANG C, FENG K, LI Z G, LU F G, HUANG J, WU Y X, CHU P K. Enhancement of high-temperature strength of Ni-based films by addition of nano-multilayers and incorporation of W [J]. Acta Materialia, 2017, 133: 55−67.

[59] WANG Y X, ZHANG S, LEE J W, LEW W S, LI B. Toughening effect of Ni on nc-CrAlN/*a*-SiN_x hard nanocomposite [J]. Applied Surface Science, 2013, 265: 418−423.

调制层厚度对 VN/TiN−Ni 纳米多层膜微观结构和力学行为的影响

程文杰[1,2]，刘 平[2]，祝新发[3]，孟 漪[3]，陆红妹[3]，Peter K. LIAW[4]，李 伟[2]

1. 汉江师范学院 物理与电子工程学院 新型功能材料制备与性能研究中心，十堰 442000；
2. 上海理工大学 材料与化学学院，上海 200093；
3. 上海工具厂有限公司，上海 200093；
4. Department of Materials Science and Engineering, The University of Tennessee, Knoxville TN 37996, USA

摘 要：采用反应磁控溅射技术，在硅基底上制备了 VN/TiN−Ni 纳米多层膜，系统研究了调制层厚度对界面结构和力学性能的影响。通过 X 射线衍射、扫描电子显微镜、X 射线光电子能谱、透射电子显微镜以及纳米压痕测试对薄膜进行了表征。结果显示，TiN−Ni 层在 VN 层上外延生长，两个子层之间形成了共格界面结构。当两个子层的调制沉积时间比(T_{TiN-Ni}:T_{VN})为 10:12 时，薄膜表现出优异的力学性能，其硬度、弹性模量、断裂韧性分别为 25.9 GPa、317 GPa 和 1.88 MPa·m$^{1/2}$。与单层 VN 薄膜相比，断裂韧性提高了约 50%，这归因于子层间共格界面的形成以及 TiN−Ni 层中相分离的促进作用。

关键词：纳米多层膜；调制层厚度；相分离；强化；断裂韧性

(Edited by Bing YANG)